Technical Report ARAED-TR-90029

AN ANALYSIS OF IMPACT INITIATION OF EXPLOSIVES AND THE CURRENTLY USED THRESHOLD CRITERIA

Barry D. Fishburn

November 1990

US ARMY
ARMAMENT MUNITIONS
& CHEMICAL COMMAND
ARMAMENT RDE CENTER

U.S. ARMY ARMAMENT RESEARCH, DEVELOPMENT AND ENGINEERING CENTER

Armament Engineering Directorate

Picatinny Arsenal, New Jersey

The views, opinions, and/or findings contained in this report are those of the author(s) and should not be construed as an official Department of the Army position, policy, or decision, unless so designated by other documentation.

The citation in this report of the names of commercial firms or commercially available products or services does not constitute official endorsement by or approval of the U.S. Government.

Destroy this report when no longer needed by any method that will prevent disclosure of contents or reconstruction of the document. Do not return to the originator.

PAGES _____

ARE

MISSING

IN

ORIGINAL

DOCUMENT

AD A

UNCLASSIFIED
SECURITY CLASSIFICATION OF THIS PAGE

REPORT DOCUMENTATION PAGE

1a. REPORT SECURITY CLASSIFICATION UNCLASSIFIED	1b. RESTRICTIVE MARKINGS
2a. SECURITY CLASSIFICATION AUTHORITY	3. DISTRIBUTION/AVAILABILITY OF REPORT Approved for public release; distribution unlimited.
2b. DECLASSIFICATION/DOWNGRADING SCHEDULE	
4. PERFORMING ORGANIZATION REPORT NUMBER Technical Report ARAED-TR-90029	5. MONITORING ORGANIZATION REPORT NUMBER
6a. NAME OF PERFORMING ORGANIZATION ARDEC, AED 6b. OFFICE SYMBOL SMCAR-AEE-W	7a. NAME OF MONITORING ORGANIZATION
6c. ADDRESS (CITY, STATE, AND ZIP CODE) Energetic Materials and Warheads Division Picatinny Arsenal, NJ 07806-5000	7b. ADDRESS (CITY, STATE, AND ZIP CODE)
8a. NAME OF FUNDING/SPONSORING ORGANIZATION ARDEC, IMD STINFO Br 8b. OFFICE SYMBOL SMCAR-IMI-I	9. PROCUREMENT INSTRUMENT IDENTIFICATION NUMBER
8c. ADDRESS (CITY, STATE, AND ZIP CODE) Picatinny Arsenal, NJ 07806-5000	10. SOURCE OF FUNDING NUMBERS PROGRAM ELEMENT NO. DL-09 / PROJECT NO. 03391 / TASK NO. / WORK UNIT ACCESSION NO.

11. TITLE (INCLUDE SECURITY CLASSIFICATION)

AN ANALYSIS OF IMPACT INITITATION OF EXPLOSIVES AND THE CURRENTLY USED THRESHOLD CRITERIA

12. PERSONAL AUTHOR(S)
Barry D Fishburn

13a. TYPE OF REPORT	13b. TIME COVERED	14. DATE OF REPORT (YEAR, MONTH, DAY)	15. PAGE COUNT
Final	FROM Jan 89 ~~TO~~ Feb 90	November 1990	50

16. SUPPLEMENTARY NOTATION

17. COSATI CODES			18. SUBJECT TERMS (CONTINUE ON REVERSE IF NECESSARY AND IDENTIFY BY BLOCK NUMBER)
FIELD	GROUP	SUB-GROUP	Impact initiation of explosives; Jet initiation of explosives

19. ABSTRACT (CONTINUE ON REVERSE IF NECESSARY AND IDENTIFY BY BLOCK NUMBER)

This work tied together published experimental and theoretical results concerning the threshold conditions for initiation of explosives during impact and/or penetration by projectiles or shaped charge jets. The shape of a projectile's tip, which may effect either pressure (if pointed) or duration (if rounded), has well known strong effects on the threshold velocity. A qualitative analysis was incorporated here that satisfactorily related these effects to results obtained with flat nosed rod impacts. Further, evidence was presented that even shaped charge jets display a significant nose shape effect, which ~~adds~~ complicates evaluating the response of explosives to jets.

There is strong, convincing evidence that for each impactor (effective) diameter, a certain threshold pressure is required for initiation. However, some (nominally) conflicting data exist and ~~are~~ were discussed.

20. DISTRIBUTION/AVAILABILITY OF ABSTRACT	21. ABSTRACT SECURITY CLASSIFICATION
☐ UNCLASSIFIED/UNLIMITED ☒ SAME AS RPT. ☐ DTIC USERS	UNCLASSIFIED

22a. NAME OF RESPONSIBLE INDIVIDUAL	22b. TELEPHONE (INCLUDE AREA CODE)	22c. OFFICE SYMBOL
I. HAZENDARI	DSN 880-3316	SMCAR-IMI-I

DD FORM 1473, 84 MAR

UNCLASSIFIED
SECURITY CLASSIFICATION OF THIS PAGE

CONTENTS

FIGURES

INTRODUCTION

Initiation of explosives via impact of projectiles or shaped charge jets has been actively discussed in numerous papers lately. The suggested criteria for initiation is that the projectile velocity squared times its diameter is a constant dependent only on the explosive. Chick (ref 1) has shown that, besides the impact shock, the flow field about a projectile passing through the explosive can also initiate detonation. If V_p is the penetration velocity, Chick suggests that $V_p^2 d$ (d=projectile diameter) is constant for this mechanism, although the constant is different than for impact initiation. Usually this bow shock initiation situation occurs because a sufficiently thick cover is on the explosive, which absorbs the impact shock. However, very small jets do not produce impact shock initiation on bare explosive, but do cause bow shock initiation. The $V_p^2 d$ value for this process is again different from both of the above values. In addition, data from reference 2 shows that there is a significant effect on $V^2 d$ from the shape of the tip of the projectile. This shape effect was also clearly recognized by Roslund et al. (ref 3) in their experiments with pointed rods. It is generally accepted that impact initiation is primarily dependent on pressure and pulse duration. The goal of this report is to relate various results reported in the literature to each other by examining pressure, duration, and other parameters of the collision.

Characterizing the Flow Caused by Impact and Penetration

A means of estimating pressures, durations, etc. from the impact of projectiles is needed. Mader et al. (ref 4) has published a set of calculations of rod impacts and steel ball impacts on several materials. It is useful to look at these results and how they compare with the usual estimating formulas for important quantities. This is shown in table 1 and discussed below:

(P_{SC}/P_H) is the ratio of the maximum centerline pressure from the computer computation compared to the value obtained by matching Hugoniots. The ratio is usually close to 1.0 except for water and the Comp B computation. This probably implies Mader et al. use different material values for water and Comp B; the values used here were taken from reference 5. The Hugoniot matching should be exact.

$(P_{stag}/.5 r_t V_p^2)$ is the ratio of stagnation pressure to dynamic pressure. Here penetration velocity is V_p as calculated from

$$\frac{V}{V_p} = 1 + \sqrt{\frac{r_t}{r_j}}$$

(incompressible hydrodynamic value). Table 1, column 5 shows this to be about the correct value, except at low velocities impacting reactive Comp B. The reaction and resulting pressure increase slows the penetration. The flat nosed rods thus have a maximum pressure coefficient of about 1.0. A problem with the ball computer calculation is that it gives V_p too high compared to experiment.

(t/(R/S)) is the duration of the impact pressure divided by the characteristic impact time. The signal speed of the relief wave behind the shock is being approximated by the shock speed. This approximation is justified by Jacob's formula for sound speed, viz

$$\frac{c}{S} = 1 + \frac{u}{S}\left[b\text{-}1\text{-}b\frac{u}{S}\right]$$

where b is from the Hugoniot, S = a + bu, and c is the speed of the head of relief wave. For all situations to be examined herein, c/S = 1 ± 0.1, so c ≈ S. The results show duration of the impact pressure is fairly well characterized by assuming the expansion propagates at the shock speed in the target or rod, whichever is larger. At higher impact velocities, the shock speed in the target should be used. The calculation for unreactive Comp B does not fit as well as the others; but, using the shock speed in the target is superior.

$(P_{CJ}/.5r_tV_p^2)$ is the ratio of detonation pressure to stagnation pressure, which indicates when reaction can be expected to have a noticeable effect on the penetration velocity.

(Ui_c/U_{i_H}) is the ratio of the interface velocity just after collision as computed and as calculated from Hugoniot matching. As it should be, it is always close to 1.0.

$(V_{p_c}/V_{p_{hy}})$ is the ratio of computer calculated penetration velocity to the incompressible hydrodynamic penetration velocity. It is close to 1.0 except in the case where reaction is occurring in the PBX 9404.

As a general observation, table 1 suggests that it is reasonable to assume the characteristic parameters associated with impact are:

$$P_s = P_H$$

$$P_{stag} = \frac{1}{2} r_t V_p^2$$

$$\frac{V}{V_p} = 1 + \sqrt{\frac{r_t}{r_j}}$$

with

$$t_{impact} = \frac{R}{S_{target}}$$

unless $S_{impactor}$ is larger.

ANALYSIS OF PBX 9404 DATA

Data on rod impact of bare PBX 9404 are reviewed in table 2. Various parameters, which have been suggested as correlating parameters, are computed and listed in the table. The work done on the explosive during impact is approximately proportional to $P_S U_i t$, which has been suggested as a correlation parameter as well as the obsequious V^2d parameter. In addition, the run to detonation at pressure P_S is given (relative to the rod diameter) as d/X_{run}, and the ratio of rod diameter to critical diameter is listed as d/d_{crit}.

The data from reference 2 are go points used to define a threshold curve. For the flat faced rods, there is not much to choose from between $P_S U_i t$ and V^2d as a correlation parameter. Note, they are not equivalent here, because t is sometimes defined in terms of target rather than impactor. If $S_{impactor}$ were always used, then they would always be equivalent. Note that the ratio of rod diameter to the run-to-detonation (X_{run}) at the impact pressure is as steady as the $P_S U_i t$ or V^2d. The round nose rods require higher velocities for initiation. Thus V^2d is about four times that for flat faced rods. The V^2d for a steel ball and for a shaped charge jet is close to that of the round nosed rods. Apparently this jet acted like the round nosed rods, not flat faced rods.

Mader and Plimbly (ref 6) modeled flat rod impact for copper, aluminum, and water. The copper calculations give a V^2d comparable with the round nosed value from experiment. The aluminum and water rods give high values. When adjusted by multiplying by rod density, viz, rV^2d (table 2, col. 20), the results fall somewhat in line. Calculations assuming aluminum and water jets, needed high impact pressures for detonation. The values of $P_S U_i t$ for these higher pressure calculations are significantly larger than seen in the experimental values listed in the table, and the aluminum and water calculations give very nearly the same high $P_S U_i t$ value. If the extrapolated values for X_{run} can be trusted, these higher pressure calculations give a (d/X_{run}) which is

also significantly higher than found elsewhere and not too consistent between aluminum and water. The aluminum calculations appear to need higher impact pressures than water, and much higher than copper, to effect detonation.

Some of the apparent differences between flat nosed and round nosed can be understood from simple geometrical considerations. The contact point (fig. 1) moves radially with speed = V/(tan b) where b measures the azimuth. At first contact, this is enormously fast compared to the shock speed in the explosive, so it resembles planar impact. However, the contact point speed drops quickly and falls below the shock speed at time $t_1 = (R/V)(1 - \cos b^*)$, where $b^* = \arctan(V/S_{target})$, if deformation of the rod is neglected. At this time, the shock effectively knows the front of the rod is rounded, and expansion will begin to proceed towards the centerline. The time for expansion to affect the centerline is thus approximately given by

$$t_{total} = R_{eq}/S_{target} + t_1$$

where

$$R_{eq} = R \sin b^*.$$

A similar treatment is given by Ferm and Ramsay (ref 7). When t_{total} is used for $P_S U_i t$, the results for the round nosed rods are closer to the $P_S U_i t$ for the flat nosed, but about 40 to 50% larger. However, $V^2 d_{eq}$ is similar to the values for flat nosed and so is (d_{eq}/X_{run}). The steel ball result of Rice and the jet result of Campbell are closer to the flat rod results when corrected for their round nose geometry. Thus d_{eq}/X_{run} for the 2.2 km/s flat rod compares within 4% to the 2.83 km/s corrected jet while the ball has a value within 10% of that of the flat rod at about the same velocity.

Some results of computer simulations of both flat and round nosed rods with a code which used a form of the LLL ignition and growth burn law are presented in reference 2. The authors state that good agreement occurred for the flat nosed rods with fair agreement for the round nosed rods. They mention that the flat nosed simulations drift towards higher threshold velocities than obtained from experiments as the projectile diameter decreases. This means the PBX 9404 is really more sensitive than indicated by the calculations for diameters less than 4 mm. The author's comments concerning the round nosed bare charge calculations seem unwarranted. Their figure 6 (ref 2), which they use to compare their data with computer results appears to have the experimental curve improperly located. If the computer results are plotted on figure 3b, reference 2, which seems to be correct, the computer results look better, with only a slight oversensitivity for the calculation at large rod diameter. No computer calculations for round nosed rods are presented at smaller diameters (less than 4 mm). Their simulations seem to agree with experiments at larger rod diameters. An interesting

observation along these lines, is that (d_{eq}/X_{run}) for the fastest flat and round nose rods as well as Campbell's shaped charge results are somewhat higher than the general value. These three cases have $V \geq 2$. Thus the data regime where the computer simulation appears to be failing does seem to have some different characteristic. What meaning can be attached to this observation is unknown.

ANALYSIS OF COMP B DATA

Comp B data are not so consistent, at least when compared between authors. Compiled Comp B data is shown in table 3. Note that not all the Comp B's are exactly the same, and the correct Hugoniots and pop plots for each type were not available. The relationships used to generate derived values are indicated.

Held's original data (ref 8), which first suggested the V^2d = constant criterion would work with shaped charges, are shown in table 3. Here, V^2d is especially steady as diameter varies. (d/X_{run}) is not quite as steady, although not too bad, while $P_S U_i t$ does not work. However, Held's value for V^2d is unusually small compared to later researchers and his value of (d/X_{run}) is very small.

Moulard's data (ref 9) includes an aluminum rod. Obviously, $P_S U_i t$ does not correlate his results. The $V_2 d$ does better, but still is not so good. Mader and Plimbly's suggestion for using r (density) to adjust between aluminum and steel rods, does not help much. However, (d/X_{run}) is fairly steady for all data. In fact, if the smallest rod is excepted, (d/X_{run}) is very steady.

Roslund quotes a threshold value for Comp B which has $V_2 d$ and d/X_{run} somewhat smaller than Moulard's. Mader and Plimbley (ref 6) reference a value $V^2d = 29$ for Comp B obtained by Campbell. Assuming Campbell used a 2 mm jet (as he did forPBX 9404) then conditions are as listed in table 3. It was found that with the PBX 9404 data that Campbell's jets behaved like round nosed rods. When the shape correction is made, Campbell's result is somewhat in agreement with other data and agrees well with Roslund's value. It is noteworthy that the difference in impact pressure for these two cases is a factor of 7.5. In fact, the jet impact pressure is above P_{CJ} for Comp B.

Chick et al. (ref 1) was the first to show two possible initiation mechanisms exist. If the impact shock is eliminated by easing the shaped charge jet into the explosive (or by a very small jet) initiation can still be caused by the flow around the tip of the jet penetration cavity, which is larger than the jet itself. Chick's bare charge result, which used a nominal 1.5 mm-diameter jet, seems to indicate the impact pressure needs to be significantly above P_{CJ} for initiation. At a just slightly smaller diameter, Held lists a threshold pressure less than P_{CJ}. There is some disagreement here. The V^2d for Chick's data is in line with Moulard's data for flat rods. Remember, Campbell's data agreed with round nose rods. If the correction for the rounded nose effect is applied to Chick's result, the V^2d_{eq} agrees with the uncorrected V^2d of Held. Once again, a confusing state of affairs. Some conditions in the bow wave flow field about Chick's jets, which initiated via this mechanism, are given. The very small jet hit bare explosive, but the impact shock failed to initiate it. The pressure in this impact appears to be enormous, and other parameters are as large as would produce impact initiation for a larger jet, with the exception of the duration. This duration is probably less than the time required for Comp B to pass through its reaction zone in a propagating detonation (about 0.02 msec). In addition, the ratio d/d_{crit} is quite small for this jet.

Threshold parameters for covered Comp B using copper and aluminum jets are given in reference 10. Upon examination of the bow shock parameters, it is seen that the largest jet has a fairly low penetration velocity, probably, at best, transonic. Chick et al. (ref 11) have presented results showing the velocity needs to be at least sonic to effect detonation. The calculated pressure associated with some of these bow shocks is very low. However, shock pressure values calculated here are much lower than those previously published by Chick et al. (ref 11). The reason for this discrepancy is due to different sources for constants in the shock Hugoniots. At present there is no way of knowing if either set of constants are appropriate for Chick's Comp B, so a preference cannot be made. The time which material spends in the subsonic "bubble" between the shock and the front of the jet can be estimated by (R/U_{bow}). Note that U_{bow} and V_p are not too different, since the bow shock is not very strong. Work done on a particle of explosive as it flows through this bubble is of order $P_{stag}V_p(R/U_{bow})$ and this quantity is listed in table 3. It has a similar magnitude and variation as $P_S U_i t$ for Moulard's impact data. The parameter $V_p^2 d$ does not correlate the data very well. Both $\sqrt{r}\ V_p^2 d$ and d/X_{run}, with X_{run} based on P_{stag}, have less variation, but are not very good either. The values for d/X_{run} are small for this bow shock case. Actually, "d" should be the diameter of the penetration cavity rather than the jet diameter used in the table, because the characteristic length for the flow field in the target really depends on the shape of the penetrating cavity. If the values in the table, about 0.3, are assumed to agree with Roslund's value, 1.16, it infers that the penetration cavity diameter is almost

four times the jet diameter. Mader et al.'s calculations for penetration into PBX 9404 show the penetration cavity may indeed be about this size. Metal rods impacting metal targets typically give ratios of cavity radius to rod radius of between 3.5 and 4.2. A model for crater formation by jet impact (ref 12) gives

$$\frac{R_{cavity}}{R_j} = \sqrt{\frac{r_j}{2f}} \; \frac{V}{1 + k\sqrt{\frac{r_j}{r_t}}}$$

which basically is the statement of the well known fact that R_{cavity}/R_{jet} is proportional to the square root of jet energy. If a value for the strength, f, of Comp B were available, then the size of the penetration cavity could be calculated. In any case, it seems probable that the cavity is large enough that both the impact shock case and the bow shock case have nearly the same value of d/X_{run} to achieve initiation.

Huang et al. (ref 13) carried out 2DE computer calculations (essentially like Mader and Plimbly's) using the Forest Fire burn rate law. For the calculations, (d/X_{run}) is constant as might be expected, since Forest Fire is strictly pressure dependent. The value of V^2d varies monatonically with velocity. However, the results give threshold velocities somewhat lower than Moulard obtained using flat rods of the same diameter as assumed in the calculations.

Pointed tips on Roslund et al. rods produce very large increases in velocity over the value for a flat nosed rod. This seems likely to be a result of reduced shock pressure in the Comp B as will be quantitatively shown below.

First, it is important to define an effectively flat nosed rod. By appealing to the considerations used to correlate round nosed rods to flat nosed, if the half cone angle is larger than $B^* = \arctan(S_{target}/V)$, then the point of contact moves faster than the shock region can expand, and the point does not affect the pressures obtained. However, if $B < B^*$, then the one dimensional impact pressure will never be obtained, and much lower shock strengths in the Comp B result. The critical angle will always be quite large, and serves to define a flat rod for impact purposes. The 60 degree angle used by Roslund et al. is less than B^*. To obtain a quantitative estimate of how the shock pressure falls off with decreasing angle, a hydrodynamic solution, valid up to the time at which the shoulder of the tip first enters the Comp B, can be obtained. This solution is a self-similar, potential solution satisfying the axial and radial momentum equations and continuity, with boundary conditions that there is no flow through the advancing tip of the rod and the velocity and pressure behind the shock satisfy the

shock jump conditions. As usual with self similar solutions, the moment of first contact of the tip with the Comp B is a singular point of the solution. The solution applies for t > 0. Further, constant density is assumed between the shock and the tip when integrating the radial momentum equation to obtain the pressure at the tip wall. Shocks of interest are strong enough to place the flow field on that portion of the P-v Hugoniot curve where density no longer changes much with increasing pressure, so this assumption seems justified. The penetration velocity of the tip is taken to be reduced from the initial rod velocity by a shock propagating back into the steel. The strength of this shock is fixed by the flow field pressure on the tip wall, which is higher than the shock pressure in the Comp B. Details are in appendix A.

How the shock pressure and wall pressure vary, according to this solution, as the nose angle decreases is shown in figure 2. How the initial rod velocity must vary to give the same shock strength in the Comp B as the tip becomes more pointed is shown in figure 3. The reference point is the 90 degree value quoted by Roslund et al. for half-inch diameter, flat nosed rods. Also shown is an analog of (d/X_{run}) = constant, where d is replaced by twice the slant height of the tip. A rationalization for this is that the expansion generated when the shoulder contacts the Comp B, must propagate approximately this distance before the entire shock region is affected. The two data points from Roslund are shown at 60 and 50 degree angles. Both curves are close together in this large angle region and the two data points sort of straddle the curves. Either curve leads to the conclusion that the shock pressure generated in the explosive using pointed rods is essentially the same as that for the flat nosed rods, even though the pointed rods have much higher velocity.

In summary, the Comp B data is not very consistent. Especially unusual is Held's data, which show Comp B to be much more sensitive than data of later researchers. Aluminum rod data demonstrates that the threshold velocity is determined by the need to reach a certain pressure in the explosive, which, of course, means (d/X_{run}) will not change when different materials are used for the impactor. This result was known previously. Howe (ref 14) cites data by Brown and Whitbread showing that the same shock pressure is required for a given size rod, independent of rod material. There appears to be disagreement with the PBX 9404 computer simulations of Mader and Plimbly, which show different pressures for different materials, although the simulations threat a significantly higher pressure regime. Superposed upon all these considerations is the great sensitivity of the impact shock to impactor shape. A strongly pointed rod might require greater than 5 km/sec to initiate Comp B via impact shock. The actual shape of the front of a jet seems to be an important variable, which has not received much attention as yet.

OTHER EXPLOSIVES

Vigil (ref15) fired small jets (0.41 mm @ 5.4 km/sec up to 0.097 mm @ 6.5 km/sec) into LX-13, PETN, PBX 9407, and tetryl. He found V^2d correlated his results and that X^2d could be plotted versus

$$\left(\frac{r_j}{r_{HE}}\right)\frac{P_{CJ}}{(r_{HE}\,d_{crit})}.$$

No physical justification was offered. He lists only one jet diameter for each explosive in his data, so not much analysis is possible.

Mader and Pimbley (ref 6) present data on shaped charge jet initiation of PBX 9502 obtained by Campbell. This data and derived quantities are shown in table 4. The impact pressures required for initiation are significantly larger than P_{CJ} for both jet diameters. Durations are short compared to the time required for reaction in a propagating detonation (about 0.4 msec). In this sense, these results are analogous to the very small jet impact on Comb B by Chick. The smaller jet diameter (4 mm) is 40% of the PBX 9502 critical diameter, which is a larger fraction of d_{crit} than in Chick's experiment. At these overdriven pressures, there is no meaning to X_{run}, so columns involving this parameter are blank. V^2d is an excellent correlation parameter between the two diameters as shown in table 4. The V^2d_{eq} does not seem to work, which again raises the question of whether these jets are round nosed or flat nosed. If the duration is computed as if the jets were flat nosed, then P_SU_it does just as well as V^2d in relating the threshold at these two diameters. Until now, P_SU_it has not been found to work very well. One physical interpretation of this parameter is it represents the blast energy in the decaying impact shock for these greatly overdriven detonations. Then the situation has similarities to the point initiation of detonation in gases, which has a rich literature (ref 16). Events observed in gases are shown schematically in figure 4. Initially, the detonations are always overdriven, but the decay of the shock can lead to detonation or complete failure, depending on the amount of initial blast energy. Based on this analogy, P_SU_it would be the parameter which determines a threshold. Perhaps two distinct regimes of impact initiation, depending on whether the impact shock builds up to detonation or decays down to detonation, should be considered. However, recall that Campbell's PBX 9404 result also had impact pressure greater than P_{CJ}, and it fit the d_{eq}/X_{run} criterion well. Further experiments are needed to clarify this point.

GREEN'S MODEL

Green (ref 17) has developed a theory for calculating threshold conditions when the rod is larger than the critical diameter of the explosive. In his model, an equivalent pressure is defined at distance x from the rod-explosive interface by

$$\frac{P_{eq}}{P_S} = \left[1 + \frac{x}{d}\right]^{-1}$$

where d is rod diameter and P_S is impact pressure. The run to detonation, X_{run}*, is calculated from pop plots based on this pressure. This value of x is compared to a distance (x + h). Here h is the distance beyond x required for an expansion, originating at the edge of the shock when it is at location x, to reach within a critical radius of the axis. The edge of the shock is determined by $d_{eq} = d + 2x$. He carries out an interactive procedure until X_{run}* is less than or equal to (x + h) to determine threshold velocity. An explicit relation for (d/X_{run}) based on impact shock pressure, different from $(d/X_{run}$*) based on P_{eq}, can be written from this model (app B).

$$\frac{d}{X_{run}} = G^G \left\{\frac{3.5 + \frac{d_{crit}}{d}}{4G - 1}\right\}^{(G - 1)}$$

where X_{run} is the pop plot run to detonation based on impact shock pressure and G is the pressure exponent in the pop plot, viz, $X_{run}P^G$ = constant. For Comp B, G = 1.3134 while for PBX 9404, G = 1.493. Thus for PBX 9404

$$\frac{d}{X_{run}} = 1.819 \left\{\frac{3.5 + \frac{1.18}{d}}{4.972}\right\}^{0.493}$$

with d in mm. The dependence on d is small. For example, if d = 1.27 mm, d/X_{run} = 1.72, while for d = 17.75 mm, d/X_{run} = 1.54. These values are close to experimental values listed in table 2 and the trend towards increasing values with smaller rod diameters exists in the data also. Values when this formula is applied to Comp B agree well with Moulard's data in table 3. The success of this formula shows, again, that relatively simple geometry considerations and the pop plots can describe impact shock initiation reasonably well and the results show Green's criterion is equivalent to (d/X_{run}) nearly constant, at least over the typical range of diameters.

RELATION TO 1-D EXPERIMENTS

Flyer plate experiments produce a flow significantly different from projectile impacts. However, it is instructive to relate X_{run} to the expansion from the rear of the flyer along the same lines as has been done for the 2-D impacts. Ramsay (ref 18) suggested a simplified treatment of this phenomena based on the same thinking as used so far to analyze projectile impacts. In a flyer plate experiment, the duration of pressure on the HE is set by the plate thickness. Call this duration t_1. Up until this moment, the shock in the HE is running up to detonation as if hit by an infinite plate. At t_1 an expansion in the HE races forward, and will eventually catch up to the shock, unless the growing rate of reaction intervenes. A simple minded approach is to calculate a time determined by the condition that the expansion just reaches the shock at the moment when the shock becomes a detonation. Thus a characteristic time of the process can be defined related to threshold conditions, viz,

$$t_1 + t_{catchup} = \frac{X_{run}}{S_{shock}}$$

which leads to

$$t_1 = \frac{U_i X_{run}}{(S_{shock})^2} \left[\frac{(b-1) - b\frac{U_i}{S_{shock}}}{1 + (b-1)\frac{U_i}{S_{shock}} - b\left(\frac{U_i}{S_{shock}}\right)^2} \right]$$

with U_i the interface velocity after collision and X_{run} the run to detonation. Results are plotted in figure 5 using data from the LLNL Explosives Handbook (ref 19), which is why only a limited range of pressures are shown. As can be seen, this simple formula gives correct order of magnitude, but does not reproduce $P_S U_i t = 1.84$ for Comp B. However, it works better for PBX 9404. At least this picture is able to give reasonable estimates of initiation requirements and so lends support to the attempt to apply this thinking to projectile impact.

Huang et al. (ref 11) also included 1-D flyer plate calculations in their paper. They do not obtain a constant $P_S U_i t$ value for Comp B, as is found from experiment, and, in fact, their $P_S U_i t$ values are about 5 to 7 times to large compared to experiment (note that the "Put" they show in their table does not use the explosive-impactor interface velocity as is normally used in correlating experiments, and when the proper $P_S U_i t$ is calculated, it is significantly larger than the experiment value). Their computer calculation does not indicate Comp B to be nearly as sensitive as experiments show. One could expect the Forest Fire model could be made to work well in this situation. It is not clear why the calculations did not produce the correct result.

CONCLUSIONS

Data in the literature describing projectile impact on bare explosives, does not present a completely consistent pattern of results. Collectively, there is no reason to expect the V^2d is really an independent correlation parameter. Another parameter, that does have a reasonable physical justification, is (d_{eq}/X_{run}) which loosely relates the size of the flow field to the distance required for detonation to be obtained. In particular, this parameter implies there is a threshold impact shock pressure, which depends on the (effective) rod diameter, for each explosive. Almost all data from the literature can be successfully interpretated with this idea. The close relationship between all the impact variables makes it hard to sort out various parameters. For example, sometimes V^2d is proportional to d/X_{run} due to the fact that "V" is approximately proportional to $1/X_{run}$. The relationships between impact pressures and "V" for a copper rod impacting Comp B and PBX 9404 are approximately:

$$P_S = 6.6208|V^2|^{0.6975} \text{ for Comp B}$$

$$P_S = 6.62735|V^2|^{0.6933} \text{ for PBX 9404.}$$

Their respective pop plots are:

$$X_{run}P^{1.3134} = 111.47 \text{ for Comp B}$$

$$X_{run}P^{1.493} = 46.93 \text{ for PBX 9404.}$$

Thus

$$V^2 = 11.40\left(\frac{1}{X_{run}}\right)^{1.092} \text{ for Comp B}$$

$$V^2 = 2.7873\left(\frac{1}{X_{run}}\right)^{0.9661} \text{ for PBX 9404.}$$

Clearly V^2 and $(1/X_{run})$ have the same behavior. The same holds true if an aluminum rod is considered, viz,

$$V^2 = 20.732\left(\frac{1}{X_{run}}\right)^{1.19} \text{ for Comp B}$$

However, such a relationship is not universal. For TATB

$$V^2 = 4.8546\left(\frac{1}{X_{run}}\right)^{0.5322}$$

and V^2d is no longer proportional to (d/X_{run}). Data for TATB only exists for the case where P_S is greater the P_{CJ}. As has been discussed, it is possible that this case has a different criterion than the case where P_S is less than P_{CJ}. At any rate $P_S U_i t$ or V^2d correlates the high pressure results satisfactorily and (d/X_{run}) fails. Data on TATB, using much larger impactors, is needed to resolve this question. Further support for d/X_{run} as correlation parameter also comes from Green's fairly successful theory. The derivation of an explicit expression of Green's criterion for threshold impact velocity shows his criteria is close to (d/X_{run}) = constant. However, it is obvious that an airtight argument for the use of this parameter cannot currently be made.

The various attempts at computer simulation of impact phenomena, while having a reasonable appearance, do not always give satisfying agreement with experimental results. This situation is unexpected, since the burning rate laws in these calculations are derived from shock impact experiments which differ from the projectile impact conditions, primarily in the duration of the shock loading. One would expect then to work. Some simulations have been successful.

There is scarce data on bow shock initiation. Chick (ref 11) has stated that the penetration rate in the explosive must be supersonic for initiation. Some of the data show penetration velocities can be fairly slow. The bow shock may be very weak at these transonic velocities. The actual strength is quite sensitive to Hugoniot parameters, so until a set of constants is universally accepted, there is some question as to what the bow shock pressure really is. Correlating the results using (d/X_{run}) where X_{run} is based on stagnation pressure, has a similar degree of spread as using $V_p^2 d$. Note that using stagnation pressure leads to

$$V_p^2 = \text{constant}\left(\frac{1}{X_{run}}\right)^{0.7614}$$

so there is no reason to expect both parameters to work equally well. The d, in the case of bow shock initiation, should be the diameter of the penetration cavity. Values of the constant needed for calculating cavity diameter from the jet diameter are not readily available. The data base is currently too meager to strongly support any correlation.

An obvious, distinguishing feature for the smallest jet, which could not produce impact initiation, is the exceedingly short duration of the shock, short compared to the duration of the reaction zone in a propagating detonation. This jet also had a diameter much less than the critical diameter.

Campbell's shaped charge jet results indicate his jets compare with round nosed rods, rather than flat nosed rods, with the exception of PBX 9502 data, which appears flat nosed. Round nosed rods are roughly equivalent to a flat nosed rod which is only 1/3 their diameter (actual fraction depends on the actual diameter) and so this is a significant effect. This raises the possibility that shaped charge jets may have large nose effects dependent on charge design or experiment setup. Previously, no consideration of this possibility has been discussed. This fact suggests a significant safety factor is needed when addressing threshold conditions for shaped charge initiation of explosives.

Table 1. Comparison of computer simulations with usual estimating formulas

V/R	Impactor	Target	P_{SC}/PH	$P_{stag}/.5rV_p^2$	tc/(R/Si)	tc/(R/St)	$P_{CJ}/.5rV_p^2$	Ui_c/Ui_H	Vp_c/Vp_{hy}
15/5	steel rod	steel	1.05	1.11	0.9	0.9		1.11	1.0
6.4/5	tantalum rod	steel	1.09	1.02	0.653	1.0		1.16	0.977
6.4/5	tantalum rod	water	1.54	1.2	0.478	1.1		1.03	1.02
6.0/6.5	steel rod	Comp B (off)	1.02	0.988	0.527	0.89		0.95	1.16
6.0/6.5	steel rod	Comp B (on)	0.916	1.28			2.05	0.95	1.14
2.0/6.5	steel rod (sub)	Comp B (off)	1.28	0.987	0.622	0.75		1.19	1.0
2.0/6.5	steel rod (sub)	Comp B (on)	1.4	3.27			18.44	1.08	0.748
1.2/6.5	steel ball (sub)	PBX 9404 (on)	1.0	6.11	0.44-0.75	1.0	22.2	0.971	0.467
1.0/6.5	steel ball (sub)	PBX 9404 (on)	0.89	2.35	0.50-0.75	1.0	32	0.898	0.905

NOTES:

Computer simulation without reaction indicated by "(off)".

Computer simulation values denoted by ( )c.

Impactor values denoted by ( )i.

Target values denoted by ( )t.

Subsonic indicated by "(sub)".

Table 2. PBX 9404 compilation

R	V	Type	Ui	Ps	Req	t_{flat}/t_{rnd}†	P_SUt	V^2d	V^2d_{eq}	X_{run}	d/X_{run}	d_{eq}/X_{run}	d/d_{crit}	Up**	P_{stag}	$\frac{R}{U_p}$	$P_{stag}U_p\frac{R}{U_p}$	Material	rV^2d	rV^2d_{eq}
Bahl et al. (ref 2)																				
0.635	2.2	flat rod	1.732	19.5		.104/	3.51	6.15	6.15	0.577	2.28	2.28	1.08					steel	48.5	48.5
0.889	1.62	flat rod	1.305	12.5		.170/	2.78	4.67	4.67	1.07	1.66	1.66	1.51					steel	36.8	36.8
1.778	1.13	flat rod	0.932	7.62		.365/	2.59	4.54	4.54	2.26	1.57	1.57	3.01					steel	35.8	35.8
3.81	0.75	flat rod	0.632	4.44		.800/	2.24	4.29	4.29	5.06	1.51	1.51	6.46					steel	33.8	33.8
5.08	0.65	flat rod	0.551	3.7		1.07/	2.18	4.29	4.29	6.67	1.52	1.52	8.61					steel	33.8	33.8
9.525	0.5	flat rod	0.428	2.66		2.03/	2.31	4.76	4.76	10.89	1.75	1.75	16.14					steel	37.6	37.6
2.2225	1.95	rnd rod	1.55	16.33	0.716	/.186	4.71	16.9	5.45	0.724	6.14	1.98	3.77					steel	133.3	43
2.54	1.7	rnd rod	1.365	13.42	0.77	/.214	3.92	14.7	4.45	0.971	5.23	1.59	4.31					steel	116	35.1
3.81	1.53	rnd rod	1.238	11.55	1.1	/.328	4.69	17.84	5.15	1.21	6.3	1.82	6.46					steel	140.8	40.6
5.72	1.21	rnd rod	0.994	8.35	1.37	/.417	3.46	16.75	4.01	1.97	5.81	1.39	9.69	/.945	0.822	6.05	4.7	steel	132.2	31.6
6.35	1.16	rnd rod	0.9555	7.88	1.47	/.448	3.37	17.09	3.96	2.15	5.9	1.37	10.76	/.900	0.745	7	4.69	steel	134.8	31.2
8.89	1.04	rnd rod	0.862	6.8	1.87	/.575	3.37	19.23	4.05	2.68	6.63	1.4	15.07	/.792	0.578	11.22	5.14	steel	151.7	32
Rice (ref 4)																				
6.5	1.125	ball	0.928	7.56	1.46	/.448	3.14	16.45	3.7	2.29	5.68	1.28	11.07	/.869	0.694	7.48	4.51	steel	129.8	29.2
Campbell (ref 6)																				
1	2.83	jet	2.18	28.4	0.372	.142/.0782	8.79/4.84	16.0	5.96	0.317*	6.31	2.35	1.69					copper	142.8	53.2
Bahl et al calculations																				
1.525	1.5	flat rod						6.68												
2.4	1.04	flat rod						5.19										steel		
3.645	0.83	flat rod						5.02										steel		
6.925	0.57	flat rod						4.5										steel		
3.55	1.44	rnd rod			0.99			14.7	4.1									steel		
5.75	1.07	rnd rod			1.38			13.17	3.16									steel		
Mader et al. calculations (ref 6)																				
1	2.5	flat rod	1.946	23.48		.153/	6.99	12.5		0.422	4.74							copper	111.6	111.6
2	2	flat rod	1.583	16.88		.345/	9.22	16		0.69	5.8							copper	142.8	142.8
1	6	flat rod	3.448	61.53		.103/	21.85	72										aluminum	200.4	200.4
2	4	flat rod	2.399	33.13		.267/	21.22	64		.252*	15.87							aluminum	178.2	178.2
2	6	flat rod	2.709	29.73		.295/	23.76	144		.296*	13.51							water	143.7	143.7

NOTES:
†duration given for flat nosed and round nosed as required.
*indicates extrapolated values X_{crit} p 1.493 = 46.93.
**velocity calculated from u = .8975Uo+.141 fit to data in ref 4.
P_{CJ} = 37 5 for PBX 9404

Table 3. Comp B compilation

R	V	Type	Ui	Ps	Req	t_{flat}/t_{rnd}	$P_s U t$	$V^2 d$	$V^2 d_{eq}$	X_{run}	d/X_{run}	d_{eq}/X_{run}	d/d_{crit}	Up	P_{bow}	P_{stag}	U_{rel}	$\frac{R}{U_{rel}}$	$P_{stag} U_{rel} \frac{R}{U_{rel}}$	X_{run}	d/X_{run}	$U_p^2 d$	$\sqrt{r}\ U_p^2 d$	Material	$rV^2 d$	$rV^2 d_{eq}$
Held Comp B (63-36) (ref 9) r = 1.72																										
0.625	2.11	jet	1.663	18.4	0.195	.097/.045	2.97/1.38	5.57	1.74	2.44	0.512	0.16	0.3125											copper	49.8	15.5
0.94	1.732	jet	1.381	13.9	0.267	.161/.068	3.09/1.31	5.64	1.6	3.51	0.536	0.152	0.47											copper	50.3	14.3
1.87	1.31	jet	1.06	9.5	0.456	.359/.131	3.61/1.31	6.42	1.565	5.79	0.646	0.158	0.935											copper	57.3	14
2.875	1	jet	0.8211	6.68	0.595	.608/.188	3.33/1.03	5.75	1.19	9.22	0.625	0.129	1.4375											copper	51.3	10.6
Moulard ISL Comp B (65-35) (ref 8) r = 1.72																										
2.5	1.88	flat rod	1.495	15.65		.411/	9.62	17.67		3.01	1.66		1.25											steel	139.4	
5	1.18	flat rod	0.965	8.33		.996/	8	13.92		6.88	1.45		2.5											steel	109.9	
7.5	0.924	flat rod	0.764	6.07		1.57/	7.28	12.8		10.45	1.44		3.75											steel	101	
7.5	1.11	flat rod	0.75	5.92		1.28/	5.68	18.5		10.79	1.39		3.75											aluminum	51.6	
Roslund Comp B (60-40) (ref 3)																										
6.35	0.896	flat rod	0.742	5.84				10.2		11	1.16													steel	80.5	
Campbell Comp B3 (60-40) (ref 6)																										
1	3.8	jet	2.876	43.8	0.394	.113/.0658	8.29/14.2	29	11.4				0.5											copper	258.8	101.7
Chick Aus. Comp B (45-55) (refs 10 and 11) r = 1.65																										
0.75	3.2	jet	2.45	33.7	0.278	.094/.0515	7.76/4.25	15.4	5.7					0.375											copper	137.4	
0.375	6	jet	4.43	91.1	0.169	.031/.021	12.5/8.47	27.4	12.3	did not impact initiate				0.1875	4.2	4.03	14.55	3.64	0.103	5.46	3.31	0.227	13.2	39.5	copper	244.5
0.75	5.2	jet	no impact					40.6							3.64	1.65	10.93	3.35	0.224	8.91	4.82	0.311	19.5	59.2	copper	362.3
1.25	5.4	jet	no impact					72.9							3.05	subsonic	7.67		0.41	9.59	7.67	0.326	22.5	38.8	aluminum	203
1.5	3.6	jet	no impact					38.9							2.52	subsonic	5.24		0.6	7.92	12.66	0.237	18.75	56.9	copper	347.1
Huang et al. calculations (ref 12) r = 1.715																										
2.5	1.4	flat rod	1.163	9.28		.537/	5.8/	9.8		4.8	1.04		5											steel	77.6	
4	1	flat rod	0.8455	5.886		.831/	4.14/	8		8.04	0.995		8											steel	63.3	
5	0.9	flat rod	0.765	5.13		1.045/	3.93/	8.1		9.4	1.06		10											steel	64.1	
6	0.8	flat rod	0.683	4.4		1.262/	3.79/	7.68		11.19	1.07		12											steel	60.8	
7.5	0.7	flat rod	0.601	3.71		1.59/	3.55/	5.4		13.57	0.884		14											steel	42.8	
9	0.6	flat rod	0.518	3.06		1.913/	3.03/	6.48		16.89	1.07		18											steel	51.3	

NOTES:

$X_{run} P^{1.3134} = 111.47$ except for Huang et al. $X_{run} P^{1.134} = 60.034$.

"no impact" cases used a cover plate to absorb the impact shock.

$S = 3.08 + 2.01U$ (ref 5) except for Huang et al. $S = 2.47 + 1.88U$.

$P_{CJ} = 29.5$ for Comp B.

Table 4. PBX 9502 compilation

R	V	Type	Ui	Ps	Req	t_{flat}/t_{rnd}	$P_s U_i t$	$V^2 d$	$V^2 d_{eq}$	X_{run}	d/X_{run}	d_{eq}/X_{run}	d/d_{cnt}	Up	P_{bow}	P_{stag}	U_{rel}	$\frac{R}{U_{rel}}$	$P_{stag} U_{rel} \frac{R}{U_{rel}}$	X_{run}	d/X_{run}	$U_p^2 d$	$\sqrt{r}\ U_p^2 d$	Material
Campbell PBX-9502 (ref 6)																								
2.98	4.47	jet (failed)	3.345	56.3	1.34																			copper
2.96	4.52	jet (failed)	3.38	57.3	1.34	.331/.220	64.1/42.6	121	54.8				0.658	3.09	subsonic	9.05		0.958	26.8	25	0.237	56.5		copper
2.94	4.59	jet (det)	3.43	58.7	1.33	.326/.217	65.6/43.7	124	56				0.653	3.14	subsonic	9.35		0.936	27.5	22.5	0.261	58		copper
2.92	4.65	jet (det)	3.472	59.8	1.33																			copper
2.075	4.94	jet (failed)	3.675	65.7	0.962																			copper
1.975	5.55	jet (failed)	4.099	78.9	0.948																			copper
1.975	5.56	jet (failed)	4.107	79.1	0.948	.194/.137	63/44.5	122	58.6				0.439	3.8	2.32	13.69	3.5	0.564	27	6.58	0.6	57		copper
1.9	5.81	jet (det)	4.281	84.4	0.923	.182/.130	66.1/47.2	128	62.3				0.422	3.98	3.23	15.02	3.55	0.535	28.5	4.88	0.78	60.2		copper
1.925	5.93	jet (det)	4.364	87.6	0.941																			copper

NOTES:
P_{CJ} = 28.5 for PBX 9502.
$S = 3.26 + 1.68U$.
$X_{run} P^{3.2258} = 30469.54$

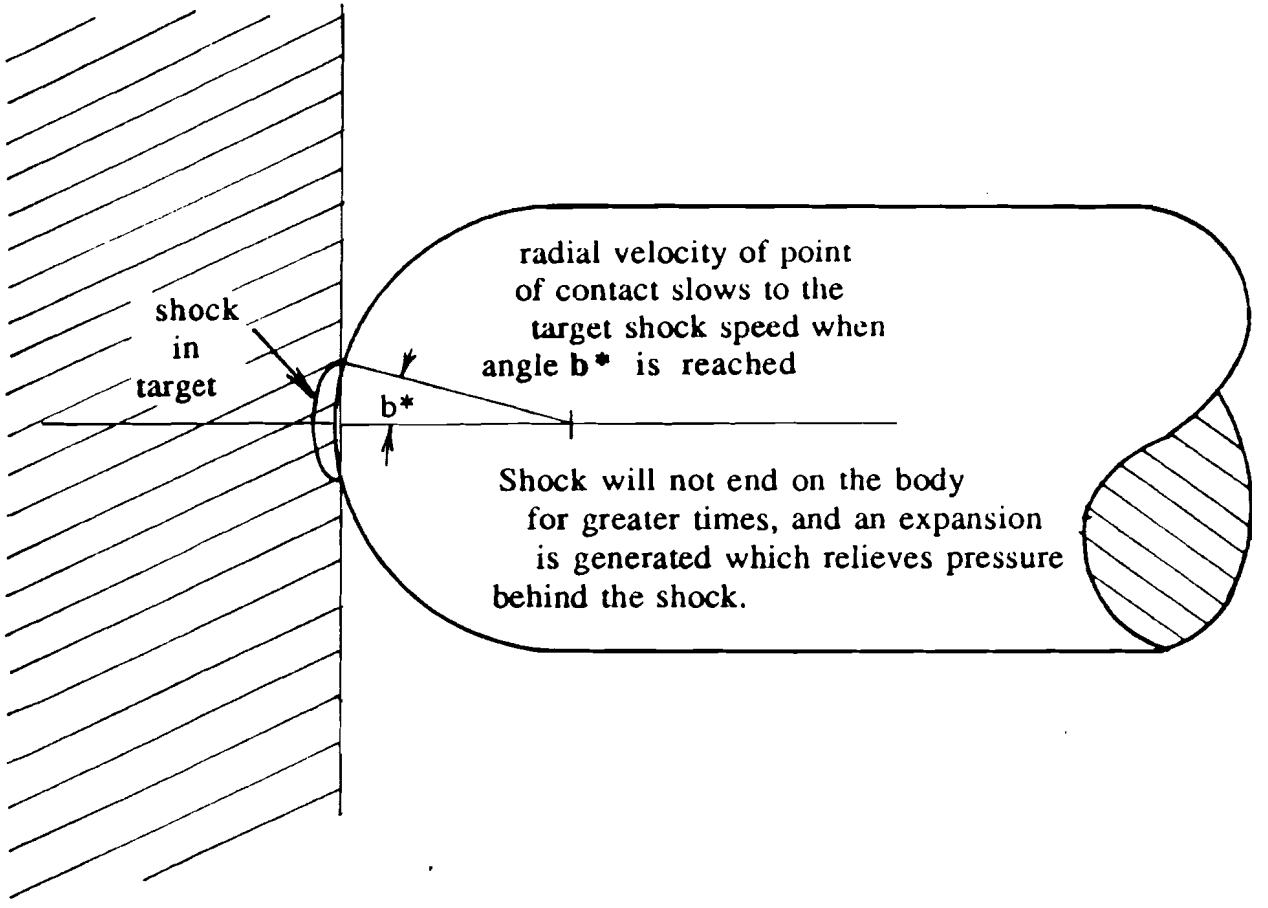

Figure 1. Impact of a round nosed rod

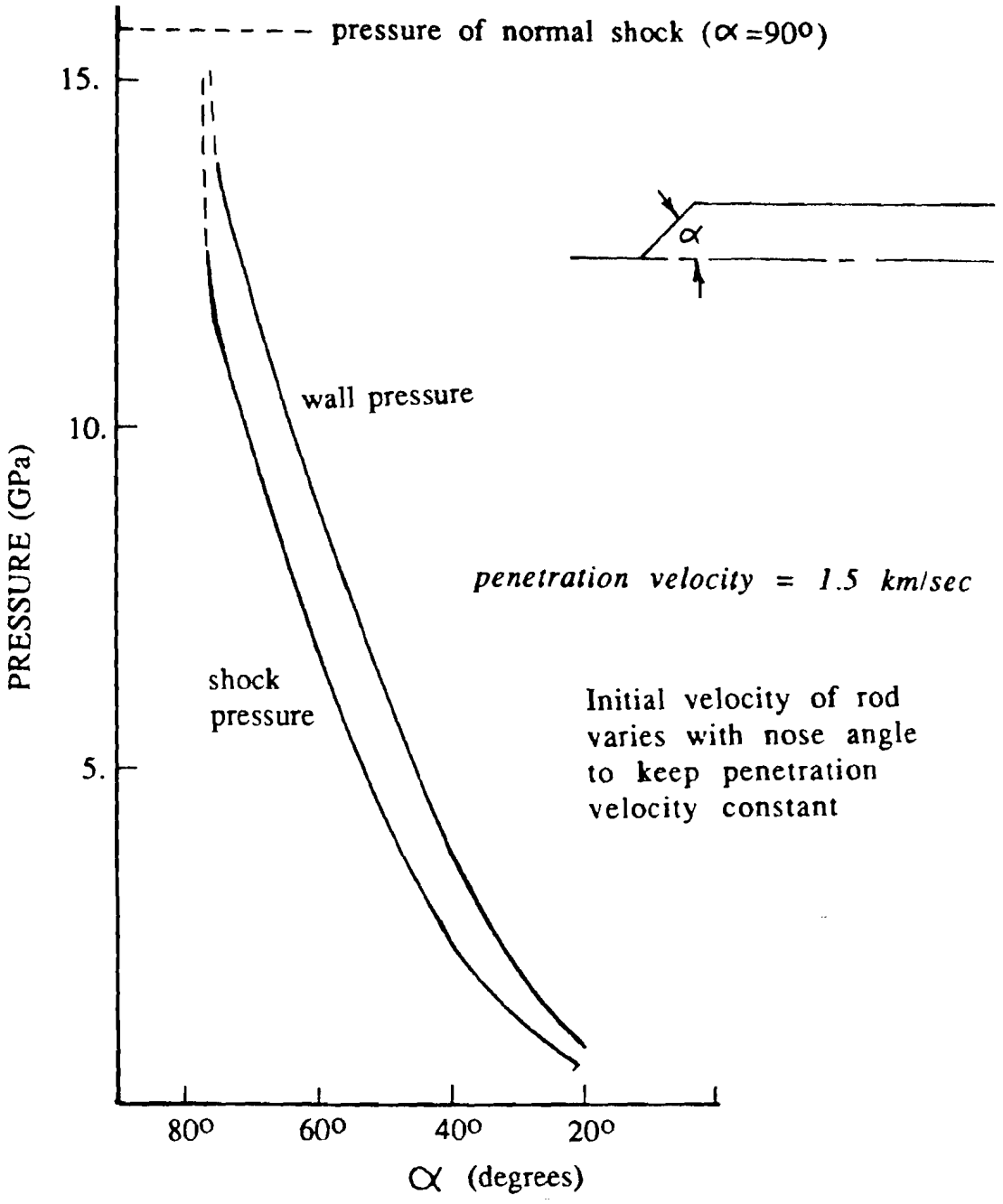

Figure 2. Shock and wall pressure versus nose angle

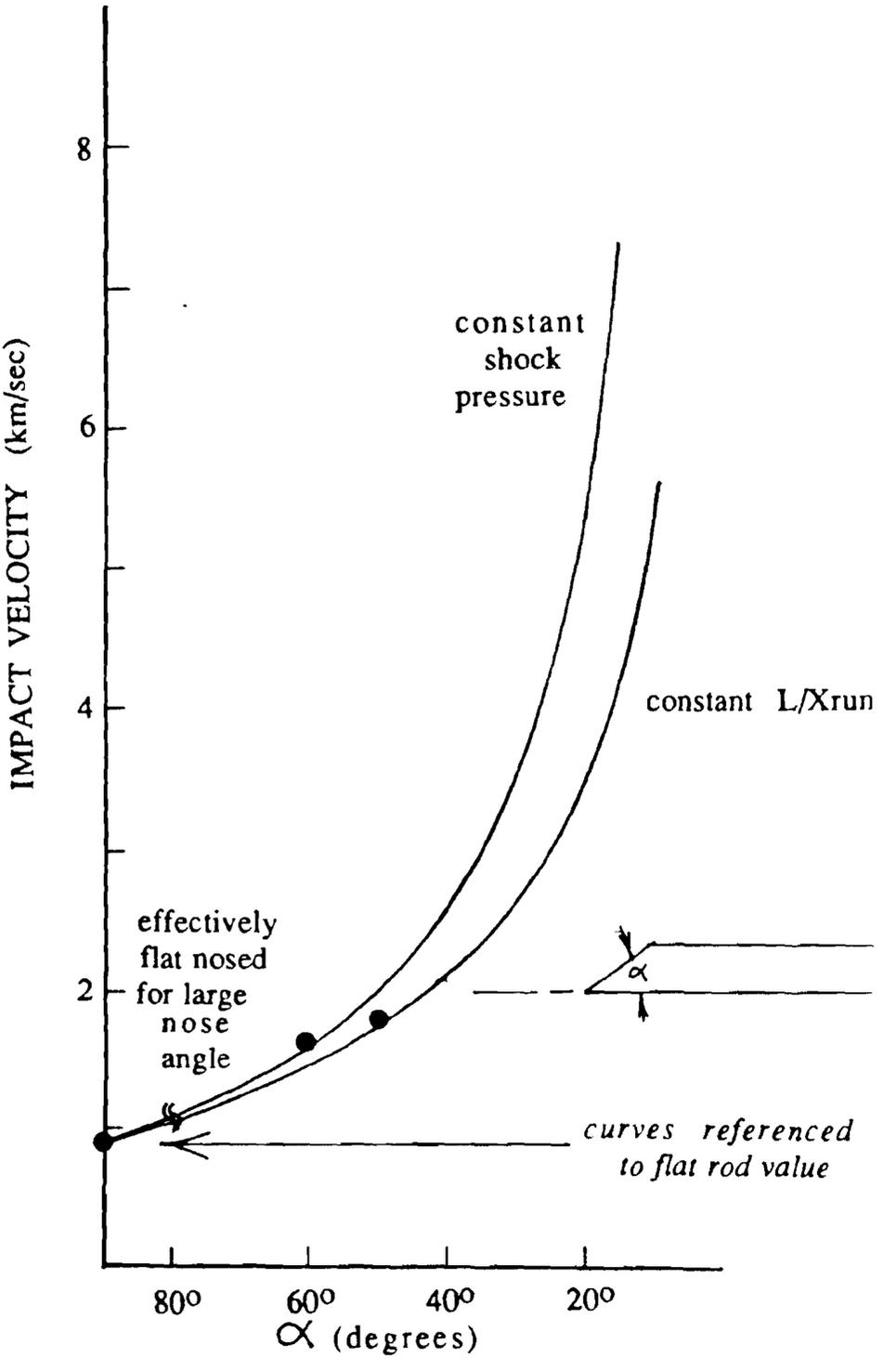

Figure 3. Impact velocity versus nose angle

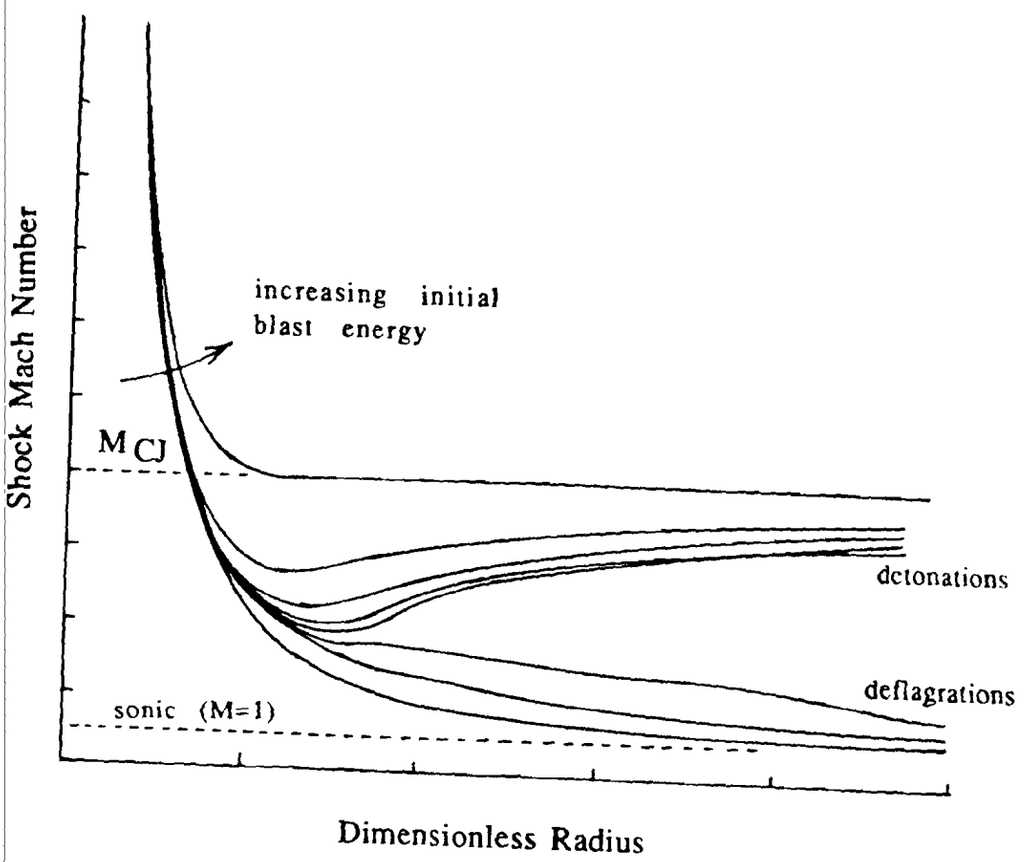

Figure 4. Point initiation of detonation in gases

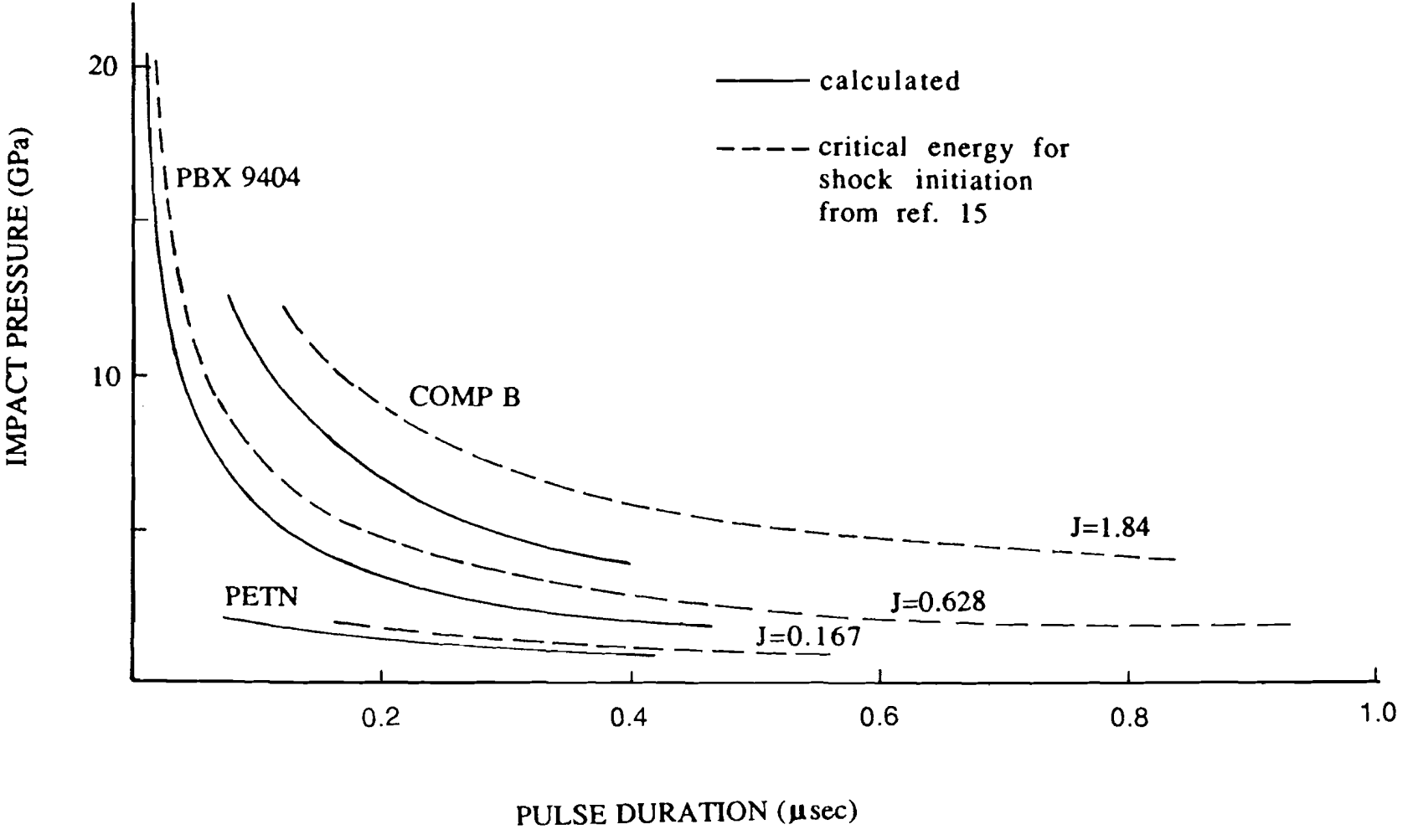

Figure 5. One dimensional initiation P-t plot

REFERENCES

1. Chick, M. C.; Macintyre, I. B.; and Frey, R. B., The Jet Initiation of Explosives, Eighth Symposium (International) on Detonation, NSWC MP 86-194, pp 318-329, July 1985.

2. Bahl, K. L.; Vantine, H. C.; and Weingart, R. C., The Shock Initiation of Bare and Covered Explosives by Projectile Impact, Seventh Symposium (International) on Detonation, NSWC MP 82-334, pp 325-335, June 1981.

3. Roslund, L. A.; Watt, J. W.; and Coleburn, N. L., "Initiation of Warhead Explosives by Projectile Impact(U)," NOLTR 73-124, Naval Ordnance Laboratory, White Oak, MD, August 1974.

4. Mader, C. L.; Pimbley, G. H.; and Bowman, A. L., "Jet Penetration of Inerts and Explosives," LA-9527-MS, Los Alamos National Laboratory, Los Alamos, NM, November 1982.

5. March, S. P., LASL Shock Hugoniot Data, University of California Press, Berkely, 1980.

6. Mader, C. L. and Pimbley, G. H., "Jet Initiation of Explosives," Los Alamos Scientific Laboratory Report LA-8647, February 1981.

7. Ferm, E. N. and Ramsay, J. B., Spherical Projectile Impact on Explosives, Ninth Symposium (International) on Detonation Preprint, vol. II, pp 662-665, August 1989.

8. Held, M., Initiating of Explosives, a Multiple Problem of the Physics of Detonation, Explosivstoffe 5, pp 98-113, 1968.

9. Moulard, H., Critical Conditions for Shock Initiation of Detonation by Small Projectile Impact, Seventh Symposium (International) on Detonation, NSWC MP 82-334, pp 316-324, June 1981.

10. Chick, M. C.; Bussel, T. J.; Frey, R. B.; and Boyce, G., Initiation of Munitions by Shaped Charge Jets, 9th International Symposium on Ballistics, Royal Military College of Science, Shrivenham, U.K., pp 2-421 - 2-430, Apr - May 1986.

11. Chick, M. C.; Bussel, T. J.; Frey, R. B.; and Bines, A., Jet Initiation Mechanisms and Sensitivities of Covered Explosives, Ninth Symposium (International) on Detonation Preprint, vol. II, pp 666-675, August 1989.

12. Szendrel, T., Analytical Model of Crater Formation by Jet Impact and its Application to Calculation of Penetration Curves and Hole Profiles, Seventh International Symposium on Ballistics, The Hague, The Netherlands, pp 575-583, 19-21 April 1983.

13. Huang, Y. K.; Starkenberg, J. J.; and Arbuckle, A. L., Some New Computed Results for Projectile-Impact Shock Initiation of Solid Explosives, Eighth Symposium (International) on Detonation, NSWC MP 86-317, pp 307-317, July 1985.

14. Howe, P. M., On the Role of Shock and Shear Mechanics in the Initiation of Detonation by Fragment Impact, Eighth Symposium (International) on Detonation, NSWC MP 86-317, p. 1152, July 1985.

15. Vigil, M. G., Explosive Initiation by Very Small Conical Shaped Charge Jets, Eighth Symposium (International) on Detonation, NSWC MP 86-317, pp. 1091-1101, July 1985.

16. Bach, G. G.; Knystautas, R.; and Lee, J. H., Initiation Criteria for Diverging Gaseous Detonations, 13th International Combustion Symposium, pp 1097-1109, 1971.

17. Green, L., Shock Initiation of Explosives by the Impact of Small Diameter Cylindrical Projectiles, Seventh Symposium (International) on Detonation, NSWC MP 86-194, pp 273-277, July 1985.

18. Ramsay, J. B., Comments on Initiation of Several Condensed Explosives by a Given Duration Shock Wave' Y. deLongueville, C. Fauquignum, and H. Moulard, Sixth Symposium (International) on Detonation, Office of Naval Research ACR-221, pp 92-94, 1976.

19. Dobratz, B. M., LLNL Explosives Handbook, Lawrence Livermore National Laboratory, UCRL-52997, March 1981.

SYMBOLS

d	Impactor diameter
d_{crit}	Explosive critical diameter
P_{CJ}	Detonation pressure
P_S	Peak Impact pressure
P_{stag}	Stagnation pressure
R	Impactor radius
R_{eq}	Impactor radius corrected for shape effects
r	Density
S	Shock speed
t	Duration
U_{bow}	Particle velocity behind a bow shock
U_i	Interface velocity
V	Initial impactor free flight velocity
V_p	Penetration velocity
X_{run}	Distance to detonation from "Pop" plots

APPENDIX A

A HYDRODYNAMIC SOLUTION FOR POINTED ROD IMPACT

The problem is to find the flow field between the shock and the advancing body (fig. A-1). Assume the flow is inviscid and incompressible so the continunity and momentum equations are

$$\frac{\partial U_r}{\partial r} + \frac{U_r}{r} + \frac{\partial U_z}{\partial z} = 0$$

$$\frac{\partial U_z}{\partial t} + U_r \frac{\partial U_z}{\partial r} + U_z \frac{\partial U_z}{\partial z} = \frac{1}{q} \frac{\partial P}{\partial z}$$

$$\frac{\partial U_r}{\partial t} + U_r \frac{\partial U_r}{\partial r} + U_z \frac{\partial U_r}{\partial z} = \frac{1}{q} \frac{\partial P}{\partial r}$$

In any cross section, A-A (fig. A-2), the body appears to have radial velocity

$$\widetilde{U_p} = V \sin \beta$$

while the actual particle velocity of a point on the body has components:

$$U_{p_r} = [U_r]_b = V \sin \beta \cos \beta$$

$$U_{p_z} = [U_z]_b = V \sin^2 \beta$$

If U_Z is considered constant, then moving A-A at this velocity reduces the problem to one of radial, unsteady flow. The phase velocity in the plane of the moving section is now

$$\widetilde{U_p} = (V - U_z) \tan \beta = V \sin \beta \cos \beta$$

Physical intuition suggests that, when looking in the section A-A, the relationship between the shock position and the body position should not change; the body is always at a certain fraction of the shock radius. Then the dimensionless radius should be defined by referring to the current shock radius, viz

$$\tilde{r} = \frac{r}{\widetilde{S}t}$$

where $\widetilde{S}$ is the phase velocity of the shock as seen in A-A and t is the time since impact began.

The simplist flow which would have an appearence as in fig. A-2 is a source flow. Let

$$U_r = \frac{c}{\tilde{r}}$$

where U_r is referenced to laboratory coordinates. On the body, where

$$\tilde{r} = \tilde{r}_p = \frac{\widetilde{U_p} t}{\tilde{S} t} = \frac{\widetilde{U_p}}{\tilde{S}}$$

so

$$U_r = \frac{c}{\tilde{r}_p} = U_p \qquad \text{or} \qquad c = \frac{\widetilde{U_p}}{\tilde{S}} U_p.$$

Shock Boundary Condition

If the true velocity of the shock is S, then the velocity components relative to the section A-A (denoted by S_R) are

$$S_{R_z} = S \sin \Omega - U_z$$

$$S_{R_r} = S \cos \Omega$$

where Ω is the shock angle (in laboratory coordinates). The radial phase velocity of the shock in section A-A is given by

$$\tilde{S} = \frac{S_R}{\cos \emptyset} \quad \text{where } S_R = \sqrt{S_{R_z}^2 + S_{R_r}^2} \quad \text{and } \tan \emptyset = \frac{S \sin \Omega - U_z}{S \cos \Omega}$$

with $\emptyset$ as the angle of the apparent shock velocity relative to A-A. Similarly, the particle velocity behind the shock in the section A-A is

$$U_{S_{AA}} = \sqrt{(U_S \cos \Omega)^2 + (U_S \sin \Omega - U_z)^2} \quad \cos \emptyset$$

where U_S is the absolute particle velocity behind the shock i.e. $S = a + b\, U_S$ is the Shock Hugoniot. This must be the velocity given by the solution, which is

$$U_r = \frac{\widetilde{U}_p U_p}{\widetilde{S}}$$

$$\frac{\widetilde{U}_p U_p}{\widetilde{S}} = \left[(U_S \cos\Omega)^2 + (U_S \sin\Omega - U_z)^2 \right]^{0.5} \cos\emptyset$$

so that

The particle velocity in the axial direction equals the axial velocity of section A-A by the assumption that U_z is constant:

$$U_S \sin\Omega = U_z$$

These can be combined to give

$$U_p \widetilde{U}_p = U_S S \cos\Omega \left[(\cos\Omega)^2 + \sin^2\Omega \left(1 - \frac{U_S}{S} \right)^2 \right]^{0.5} \qquad (1)$$

Body Boundary Condition

At the body, there is no flow through the wall, but, there can be slip because of the inviscid assumption. Let the direction of the particle velocity at the wall be given by Y (fig. A-3). Then in section A-A

$$U_{AA} = \hat{u} \cos\left(Y - (90^\circ - \beta) \right) = U_p$$

while

$$U_z = \hat{u} \sin\left(Y - (90^\circ - \beta) \right)$$

where $\hat{u}$ is the magnitude of the particle velocity at the wall. Let the normal velocity of the wall be denoted by U_w so that $U_w = V \sin\beta$. Then $\hat{u} \sin Y = U_w$. With these, the condition of no flow through the wall becomes

$$\widetilde{U}_p = V \left\{ 1 - \frac{\sin\beta}{\sin Y} \sin\left(Y - (90^\circ - \beta) \right) \right\} \tan\beta \qquad (2)$$

Equations (1) and (2) can be combined to give

$$V\frac{\tan\Omega}{\cos\Omega}\left\{1-\sin\Omega\frac{\sin\beta}{U_w}\frac{S-a}{b}\right\}\tan\beta = S\left[1+\left(\frac{a}{S\,b}\right)^2\tan^2\Omega\right]^{0.5}\tan\left(\gamma-(90^\circ-\beta)\right) \tag{3}$$

The shock angle can be retrieved from the particle velocity components at the shock:

$$\sin\Omega = \frac{U_{S_x}}{U_S} = \frac{U_z}{U_S} = \frac{\frac{U_w}{\sin\gamma}\sin\left(\gamma-(90^\circ-\beta)\right)}{\left(\frac{S-a}{b}\right)} \tag{4}$$

since U_z is uniform.

With equations (3) and (4) one can find the shock velocity for any assumed value of Ω. There exists a value of Ω , Ω^*, which gives a minimum in shock velocity for given rod velocity and tip angle. Again, by physical intuition, it is assumed that Ω^* is the value which will actually occur. This "minimum shock pressure assumption" is an additional assumption which must be envoked to give a unique solution.

Pressure on the Body

The radial momentum equation is integrated to obtain the pressure on the wall. Thus, if the density is assumed constant for the integation,

$$P = -q\,c\left(\tilde{S}\ln\tilde{r} + \frac{c}{2}\frac{1}{\tilde{r}^2}\right) + K \tag{5}$$

At the shock ($\tilde{r} = 1$)

$$P_S = -q\,c\left(\frac{c}{2}\right) + K$$

$$K = q_0 S\left[U_S + \frac{1}{2}\frac{1}{S-U_S}\left(\frac{\tilde{U}_p U_p}{\tilde{S}}\right)^2\right]$$

or

where q_0 is the initial density (q is the value after the shock, which is assumed constant for the integration). Manipulation of the

kinematic condition at the shock can be used to replace the expression in brackets to give

$$K = q_0 U_S S\left[1 + \frac{1}{2}\frac{U_S}{S - U_S}\frac{\cos^2\Omega}{1 + \left(1 - \frac{U_S}{S}\right)^2 \tan^2\Omega}\right]$$

also,

$$c\tilde{S} = U_S \cos^2\Omega\left[1 + \left(1 - \frac{U_S}{S}\right)^2 \tan^2\Omega\right]^{0.5}$$

$$c^2 = \frac{U_S \cos\Omega}{\sqrt{1 + \left(1 - \frac{U_S}{S}\right)^2 \tan^2\Omega}}$$

$$q = q_0 \frac{S}{S - U_S}$$

are needed to evaluate pressure using equation 5.

The position of the wall can be found from

$$\tilde{r}_p = \frac{\tilde{U}_p}{\tilde{S}} = \frac{c}{U_p} = \frac{c \sin Y}{U_w \cos\left[Y - (90^\circ - \beta)\right]}$$

This wall pressure drives a shock into the rod whose first order effect is to slow the velocity of the rod relative to the target explosive. That is, V in this development, is related to the original velocity of the rod, V_o, through the shock jump conditions in the rod necessary to give a pressure equal to the wall pressure from the flow field. A simple iterative procedure can be used to find the correct shock strength in the rod which produces V such that the flow field pressure on the wall matches that produced by the shock. No deformation of the rod is considered in this approximation.

List of Symbols

a,b	constants in the shock Hugoniot $S = a + b\ U_S$
q	density
S	shock velocity
U	particle velocity
U_S	velocity induced by the shock
U_W	velocity normal to wall = $\hat{u} \sin Y = V \sin ß$
$\hat{u}$	magnitude of particle velocity at the wall
V	impactor velocity (shock in impactor reduces velocity from initial free flight value without changing nose angle)
Y	angle between wall and particle velocity at wall
ß	nose half angle
Ø	angle between shock velocity relative to section A-A (laboratory S minus z velocity of A-A) and the normal to the collision centerline
Ω	shock angle
Ω*	shock angle which gives minimum shock pressure
$\tilde{(\ )}$	value as seen in a cross section view

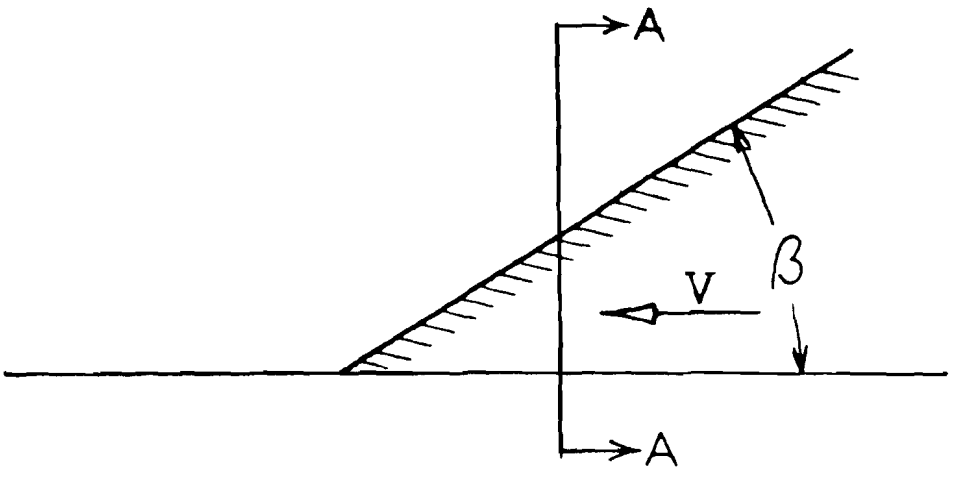

Figure A-1. Nose angle

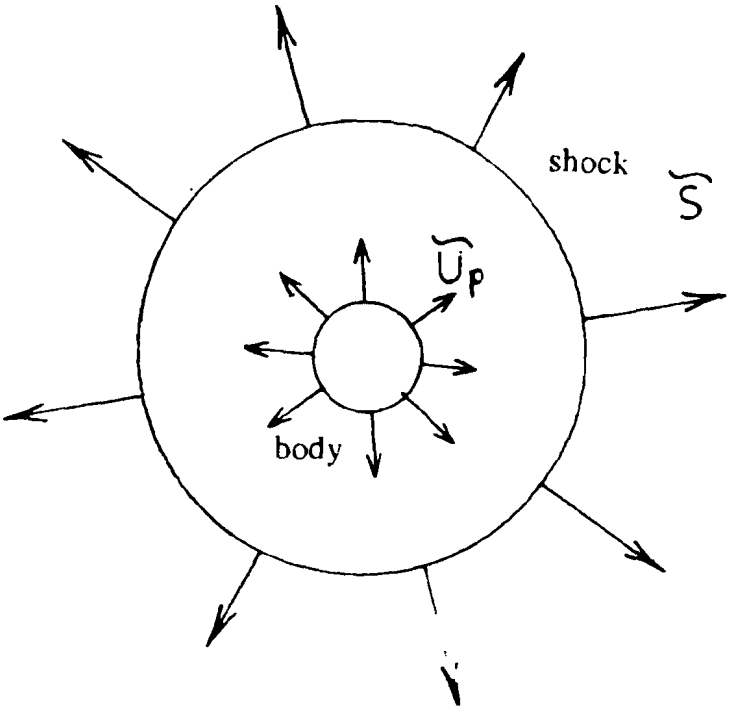

Figure A-2. Velocities seen in cross section A-A

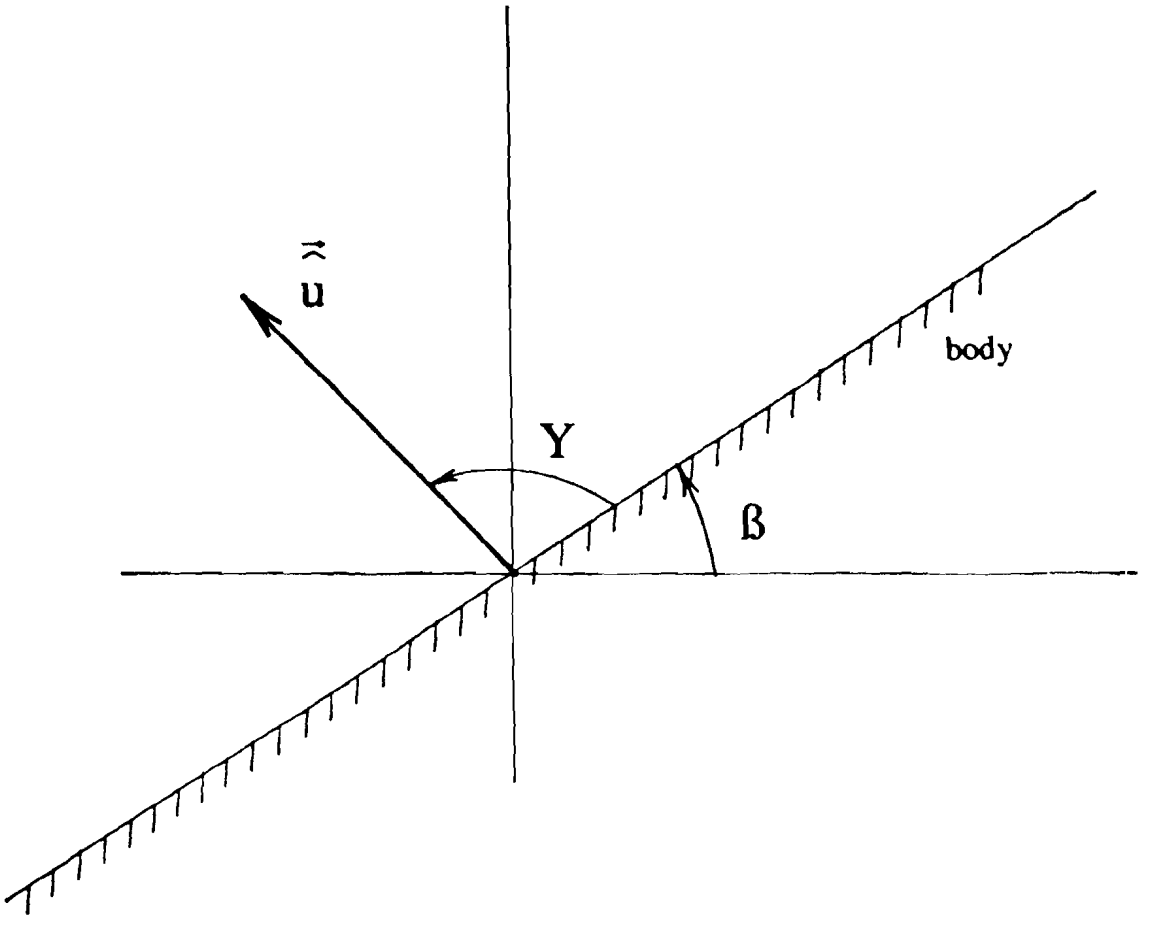

Figure A-3. Wall velocity

APPENDIX B

GREEN'S CRITERION

Green calculates an equivalent pressure as a function of the distance into the target as

$$P_{eq} = \frac{P_S}{1 + \left(\frac{x_i}{d}\right)}$$

and then defines $X_{run} = K P_{eq}^{-G}$ from the appropriate Pop plot. He assumes that at some point he has used up x_i of the X_{run} * (based on P_{eq}). An expansion comes in from d_{eq} at 45°, which will cause failure of the detonation if it comes within $0.5\ d_{crit}$ of the axis before the remaining X_{run} * is used up. The distance beyond x_i until the expansion hits $0.5\ d_{crit}$ is § = $0.5(d_{eq} - d_{crit})$. By the geometry of the 45° lines, $d_{eq} = 0.5(d_{eq} + 2x_i - d_{crit})$. The threshold condition is thus

$$K\left[\frac{P_S}{1 + \left(\frac{x_i}{d}\right)}\right]^{-G} \leq x_i + \frac{1}{2}\left(d + 2x_i - d_{crit}\right).$$

If a solution exists for this expression when the "≤" is replaced by "=", then Green's criterion is met.

Define

$$F_1 = K P_S^{-G}\left[1 + \frac{x_i}{d}\right]^G$$

$$F_2 = \frac{d}{2}\left[\left(1 - \frac{d_{crit}}{d}\right) + 4\frac{x_i}{d}\right].$$

If $K P_S^{-G} \leq \frac{d - d_{crit}}{2}$, then one always has a solution, as shown in figure B-1, since > G ≥ 1 for all usual explosives. The minimum impacting velocity is associated with the highest possible value for $Xrun_o$ (based on P_S). This minimum condition is illustrated in figure B-2. The solution point, $\tilde{x}_i$, occurs where

$$F_1 = F_2 \quad \text{and} \quad \dot{F}_1 = \dot{F}_2,$$

which can be manipulated to give

$$\frac{d}{x_{run_o}} = G^G \left[\frac{3.5 - \frac{d_{crit}}{d}}{1 - 4G} \right]^{(G-1)}$$

where X_{run_o} is the runup distance based on P_S (the impact shock pressure).

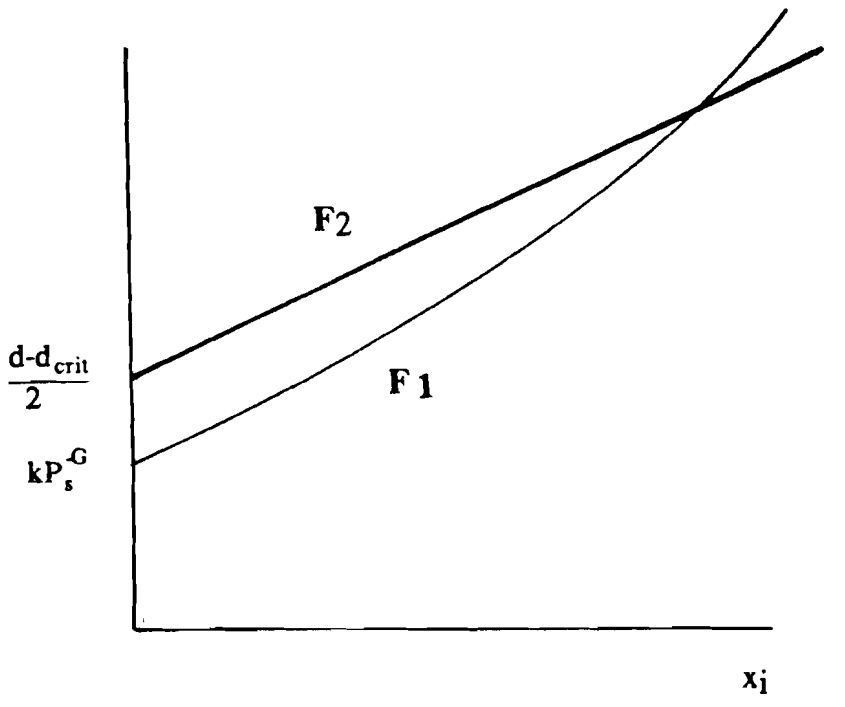

Figure B-1. General case

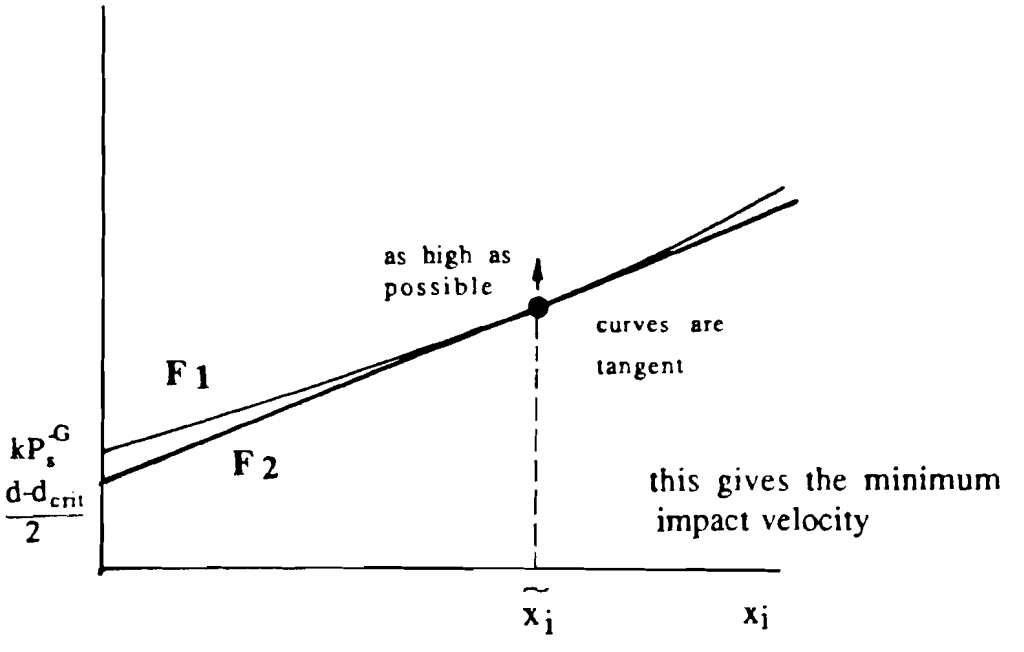

Figure B-2. Limiting case

DISTRIBUTION LIST

Commander
Armament Research, Development and Engineering Center
U.S. Army Armament, Munitions and Chemical Command
ATTN: SMCAR-IMI-I (5)
SMCAR-CO
SMCAR-TD
SMCAR-SF
SMCAR-AEE (3)
SMCAR-AEE-W (3)
SMCAR-AEF-C, R. A. Chevalaz
SMCAR-AEE-W(W), B. Fishburn (3)
SMCAR-AEE-BR (3)
SMCAR-AEE-BP
Picatinny Arsenal, NJ 07806-5000

Commander
U.S. Army Armament, Munitions and Chemical Command
ATTN: AMSMC-GCL (D)
Picatinny Arsenal, NJ 07806-5000

Administrator
Defense Technical Information Center
ATTN: Accessions Division (12)
Cameron Station
Alexandria, VA 22304-6145

Director
U.S. Army Materiel Systems Analysis Activity
ATTN: AMXSY-MP
Aberdeen Proving Ground, MD 21005-5066

Commander
Chemical Research, Development and Engineering Center
U.S. Army Armament, Munitions and Chemical Command
ATTN: SMCCR-MSI
Aberdeen Proving Ground, MD 21010-5423

Commander
Chemical Research, Development and Engineering Center
U.S. Army Armament, Munitions and Chemical Command
ATTN: SMCCR-RSP-A
Aberdeen Proving Ground, MD 21010-5423

Director
Ballistic Research Laboratory
ATTN: AMXBR-OD-ST
AMSMC-BLI-A, T. Minor
SLCBR-TB-EE, R. Frey
Aberdeen Proving Ground, MD 21005-5066

Chief
Benet Weapons Laboratory, CCAC
Armament Research, Development and Engineering Center
U.S. Army Armament, Munitions and Chemical Command
ATTN: SMCAR-CCB-TL
AMSMC-DS
Watervliet, NY 12189-5000

Commander
U.S. Army Armament, Munitions and Chemical Command
ATTN: SMCAR-ESP-L
Rock Island, IL 61299-6000

Director
U.S. Army TRADOC Systems Analysis Activity
ATTN: ATAA-SL
White Sands Missile Range, NM 88002

Commander
Naval Surface Warfare Center
ATTN: Code 101, Les Roslund
Naval Surface Warfare Center
White Oak
Silver Spring, MD 20903-5000

Hercules Aerospace Ordnance Group
111 Howard Boulevard
Suite 200
Mt. Arlington, NJ 07856

Atlas Powder Company
ATTN: John J. Mullay
P.O. Box 271
Tamaqua, PA 18252

ARMTEC Defense Products, Inc.
ATTN: J. Haley
85-901 Avenue 53
P.O. Box 848
Coachella, CA 92236

Hercules/Kenvil
ATTN: H. Ziegler
Hercules Road
Kenvil, NJ 07847

Veritay Technology, Inc.
ATTN: E. Fisher
4845 Millersport Highway
P.O. Bpx 305
East Amherst, NY 14051-0305

Director
Indiana Army Ammunition Plant
ATTN: SMCIN-CA (M. Sievers)
Charlestown, IN 47111-9667

Director
Radford Army Ammunition Plant
ATTN: SMCRA-EN, J. Pierce
Radford, VA 24141-0298

Commander
U.S. Army Missile Command
ATTN: AMSMI-RD-SS, J. P. Billingsley
Redstone Arsenal, AL 35898-5270